Aging and Disease
www.aginganddisease.org
Early access date: December 14, 2025
http://dx.doi.org/10.14336/AD.2025.1224

Original Article

Pharmacological Activation of Mitophagy Confers Neuroprotective Benefits for Amyotrophic Lateral Sclerosis

Sen Huang[1#], Ang Li[2#], Yixia Ling[2], Xinyu Yang[1], Jiayu Wang[2], Jing Yuan[1], Dajiang Qin[2*], Xiaoli Yao[1*]

[1]Department of Neurology, The First Affiliated Hospital, Sun Yat-sen University; Guangdong Provincial Key Laboratory of Diagnosis and Treatment of Major Neurological Diseases; National Key Clinical Department and Key Discipline of Neurology, Guangzhou, China. [2]Guangdong Engineering Technology Research Center of Biological Targeting Diagnosis, Therapy and Rehabilitation, The Fifth Affiliated Hospital, Guangzhou Medical University, Guangzhou, China.

[Received September 28, 2025; Revised November 20, 2025; Accepted November 24, 2025]

ABSTRACT: Amyotrophic lateral sclerosis (ALS) is a rare and devastating neurodegenerative disease characterized by the progressive degeneration of motor neurons in the brain and spinal cord, for which no cure currently exists. Previous studies have shown that abnormal mitochondrial homeostasis and defective mitophagy occur in neurodegenerative diseases, including ALS. Here, we provide evidence that PINK1–Parkin-dependent mitophagy is impaired in multiple ALS mouse models, including the SOD1^{G93A}, TDP43^{A315T}, and rNLS8 strains, leading to the accumulation of damaged mitochondria in affected motor neurons. These findings suggest that mitophagy may be a druggable target for ALS treatment. A classical mitophagy agonist, urolithin A (UA) was used in this study. UA-induced mitophagy antagonizes ALS pathologies in the ALS SOD1^{G93A} transgenic *C. elegans* model in a pink-1 (PTEN-induced kinase 1)- and pdr-1 (Parkinson's disease-related 1)-dependent manner. Furthermore, pharmacological activation of mitophagy by UA improves locomotor behavior, delays motor neuron degeneration and reduces neuroinflammation in ALS SOD1^{G93A} transgenic mice. In conclusion, our results establish impaired mitophagy as a hallmark of ALS motor neuron degeneration and demonstrate that its pharmacological activation offers a neuroprotective strategy with therapeutic potential.

Keywords: Amyotrophic lateral sclerosis, mitophagy, motor neuron, PINK1–Parkin

INTRODUCTION

Amyotrophic lateral sclerosis (ALS), also known as Lou Gehrig's disease, is a rare, progressive, and fatal neurodegenerative disease. ALS affects motor neurons in the brain and spinal cord, leading to progressive muscle weakness and atrophy, eventually resulting in death due to respiratory failure [1]. Riluzole, a glutamate antagonist, and Edaravone, a free radical scavenger, are the only approved drugs for ALS treatment by FDA in 1995 and 2017 [2, 3]. These therapeutic drugs provide symptomatic relief but are unable to cure and/or delay the progression of ALS. Therefore, there is a dire need for novel therapeutic strategies to counter ALS.

ALS pathogenesis remains unclear. It is generally believed that ALS is caused by both genetic and environmental factors, and a gene–time–environment interaction model was proposed by some researchers [4]. Since the first pathogenic gene of ALS, superoxide dismutase 1 (*SOD1*), was discovered in 1993 [5], more than 120 genetic mutations have been associated with the pathogenesis and development of ALS. Furthermore,

***Correspondence should be addressed to:** Dr. Xiaoli Yao, The First Affiliated Hospital, Sun Yat-sen University, Guangzhou, China. Email: yaoxiaol@mail.sysu.edu.cn; Dr. Dajiang Qin, The Fifth Affiliated Hospital, Guangzhou Medical University, No.621 Gangwan Road, Guangzhou, China. Email: qin_dajiang@gzhmu.edu.cn. [#]These authors contributed equally to this study.

various cellular functions are involved in the pathogenesis of ALS, including mitochondrial homeostasis, axonal transport, DNA repair, neuroinflammation, excitability, and oxidative stress [6], and can be used as potential therapeutic targets.

Mitochondria, the cell's energy factory, are crucial for cellular processes such as metabolism, energy conversion, calcium regulation, and oxidative stress regulation [7]. Cells maintain mitochondrial homeostasis through mitochondrial biosynthesis and degradation [8]. Mitochondrial degradation, also known as mitophagy, is a special macroautophagy process. During mitophagy, impaired mitochondria are wrapped by mitophagosomes, a double-membrane structure, which fuse with lysosomes for degradation [9]. Mitophagy can occur through the PINK1–Parkin (E3 ubiquitin ligase) and receptor-mediated pathways. In the PINK1–Parkin pathway, PINK1 anchors on the outer mitochondrial membrane, where it recruits and activates Parkin and phosphorylates ubiquitin at Ser65 (pSer65-Ub). Activated Parkin ubiquitinates the outer mitochondrial membrane proteins and enhances mitophagy signals [10]. Finally, mitophagy receptors recognize ubiquitinated mitochondrial proteins, and the microtubule-associated protein 1 light chain 3 is recruited to the mitochondria to assemble mitophagosomes, which induce the mitochondrial degradation process.

Mitophagy activation represents the most efficient arm of the mitochondrial quality control system, while a defective mitophagy flux has been generally associated with defective mitochondrial accumulation in various parts of neurons [11]. It has been suggested that mitochondrial dysfunction and abnormal mitochondrial homeostasis are vital pathogenic factors of ALS [12]. In the $SOD1^{G93A}$ mouse model, mitochondrial vacuoles and abnormal mitochondrial metabolism were found in motor neurons in the early symptomatic stages of the disease [13, 14]. However, the level of mitophagy in motor neurons and whether mitophagy activation can deliver a neuroprotective effect in ALS remain unclear. Previous research on neuromuscular junctions (NMJs) in motor neurons of $SOD1^{G93A}$ has shown that many damaged mitochondria were accompanied by abnormal mitophagosome reduction [15]. Therefore, mitophagy induction may be a therapeutic target for ALS, as it has been shown to deliver a neuroprotective effect in many neurodegenerative disease models [9]. Many ways to activate mitophagy have been reported, including exercise, nutritional interventions, and pharmacological approaches. Several small-molecule compounds, such as urolithin A (UA) and NAD, can induce mitophagy [16]. UA is a natural metabolite of ellagitannins (ET) in pomegranates and nuts after intestinal metabolism that induces potent mitophagy activity both *in vitro* and *in vivo* [17]. It was reported that UA can induce mitophagy without damaging normal mitochondria, has a broad range of safe dosages [18], and can permeate the blood–brain barrier [19, 20]. Therefore, this study aimed to investigate the hypothesis that impairment of PINK1 – Parkin-dependent mitophagy is a common pathogenic mechanism in ALS and to evaluate the therapeutic potential of pharmacological mitophagy activation in *C. elegans* and mouse ALS models.

MATERIALS AND METHODS

Cell culture

Mito–Keima–YFP–Parkin and YFP–Parkin HeLa cell lines were cultured in DMEM high-glucose medium (Gibco) containing 10% fetal bovine serum (Gibco) and 0.1% Mycoplasma Prevention Reagent (Transgene) and cultured at 37°C under 5% CO_2. For gene silencing experiments, cells were transfected overnight with 50 pmol siRNA (*si-pink1*: 5'-GCCGCAAAUGUGCUUCA UCUAdTdT-3') using Lipofectamine 3000 (Thermo Fisher).

Parkin translocation detection

YFP–Parkin HeLa cell line was plated in 96-well plates at approximately 8,000 cells per well. After incubating overnight at 37°C, the medium was replaced with a medium containing the test compound, and the cells were further incubated for an additional 24 hours. Subsequently, four randomly selected fields per sample were assessed using a high-content imaging system.

Flow cytometry

The mitophagy index was assessed in Mito–Keima–YFP–Parkin HeLa cell lines Cells were harvested with trypsin and analyzed using a flow cytometer (BD LSRFortessa X-20) equipped with 405-nm and 561-nm lasers. The lysosomal mito–Keima-indicated mitophagy index was detected using dual-excitation radiometric pH measurements at 405 nm (pH 7) and 561 nm (pH 4) with 695 nm and 670 nm emission filters, respectively. A minimum of 10,000 events were counted and analyzed using Diva software (BD Biosciences). Mitochondrial membrane potential (MMP) was assessed by staining the cells with 1× TMRE (Beyotime) for 15 minutes, and mitochondrial reactive oxygen species (ROS) level was assessed by staining the cells with 1× MitoSOX (Invitrogen) for 15 minutes. The cells were washed twice, harvested with trypsin, and analyzed by flow cytometry. A minimum of 10,000 events were counted. Data were analyzed using FlowJo v10.0.

Real-time quantitative PCR (qPCR) analysis of mitochondrial DNA content

Mitochondrial DNA (mtDNA) content was assessed using the human mtDNA monitoring primer set (7246, Takara). Briefly, cellular DNA was extracted from treated HeLa cells using the DNeasy Blood and Tissue Kit (69506, Qiagen). Subsequently, the mitochondrial *ND1* and *ND5* genes and the nuclear *SLCO2B1* and *SERPINA1* genes were utilized as mtDNA and nuclear (nDNA) markers, respectively, and their levels were quantified using a CFX96 real-time PCR detection system (Bio-Rad) with HiEff qPCR SYBR Green Master Mix (11202ES08, Yeasen).

Assessment of ATP production

ATP content was estimated in 10,000 cells per well in 96-well plates using the CellTiter-Glo assay (G7570, Promega) according to the manufacturer's instructions. ATP content was evaluated at baseline and 24 hours after UA treatment.

C. elegans strains

C. elegans strains were maintained at 20℃ on *Escherichia coli* OP50 using standard feeding methods. Bristol strain N2 nematodes were used as the standard non-transgenic wild-type worms. The transgenic strains ngIs19 (*unc-25p*::GFP) and ngIs27 (*unc-25*p::G93A SOD1) were kindly provided by Prof. Le Weidong. The mutant $SOD1^{G93A}$ protein was overexpressed in the motor neurons of N2 nematodes. Compared to wild-type nematodes, $SOD1^{G93A}$ nematodes, which are commonly used as a model organism for ALS [21], exhibited decreased body swing frequency, an increased proportion of paralysis, shorter survival, and a higher loss of motor neurons. The TU3401 nematodes, expressing the pan-neuronal mitophagy reporter (mt-Rosella biosensor) to monitor the level of mitophagy and neuronal RNAi, were kindly provided by Prof. Evandro Fei Fang. The list of strains used in this study is shown in Supplementary Table 1.

Drug administration to *C. elegans* nematodes

UA was purchased from Topscience (CAS 1143-70-0). UA or an equal volume of DMSO was directly added to the melted nematode growth medium (NGM) before pouring it into the plates. Nematodes were treated from either the egg or the L4 stage.

Toxicity assay in *C. elegans*

The wild-type N2 *C. elegans* strain was used to determine the safe dose of UA in a toxicity assay. Ten 1-day-old nematodes were placed on NGM plates with OP50 containing UA (25, 50, 75, or 100 μM) or not (vehicle) for one hour after laying. The number of eggs was counted after removing the adults. Subsequently, we counted the number of L1 larvae and unhatched eggs to check egg hatching efficiency. The number of L4 larvae was counted on day 2, and the number of 1-day-old adult nematodes was counted on day 3.

Neuronal mitophagy detection in *C. elegans*

Transgenic nematodes expressing a pan-neuronal mitophagy reporter (mt-Rosella biosensor) were used to assess the mitophagy level based on the ratio between pH-sensitive GFP and pH-insensitive DsRed. UA or equal-volume DMSO was added to the melted NGM from egg hatching before pouring it into the plates. On day 1, the nematodes were paralyzed by levamisole and imaged using a confocal microscope at 10× and 40× magnifications.

Motor neuron counting in *C. elegans*

Nematodes were treated with UA or vehicle from egg hatching. One-day-old adult nematodes were immobilized in 5 mM sodium azide in M9 buffer on 2% agar pad slides. The number of motor neurons in *C. elegans* was counted and analyzed on days 2, 4, and 8. Images were acquired using a confocal microscope, examining 20 nematodes from each strain.

Behavior and lifespan analysis in *C. elegans*

Nematodes were treated with UA or vehicle from egg hatching. One-day-old adult nematodes were transferred to 20 μL M9 buffer and imaged. The number of swimming waves was recorded for 30 seconds. Nematode paralysis was considered if they moved their noses but failed to move their bodies when their noses were trapped in a platinum worm picker. The paralysis time per nematode was recorded daily. Experiments were performed in triplicate with 20 nematodes per plate. For the survival analysis, L4 stage nematodes were treated with 100 μM UA or vehicle and counted daily from Day 1 until death. Nematodes were considered dead if they did not respond to external stimuli.

RNA interference by feeding

C. elegans were treated with RNAi as previously reported [22]. Briefly, nematodes were co-cultured with bacteria engineered to facilitate knockdown of *pink-1* or *pdr-1* in

C. elegans. Engineered bacteria were grown in LB media in the presence of 50 mg/mL ampicillin and added to NGM plates containing 1% ampicillin and 1% isopropyl β -D-1-thiogalactopyranoside (IPTG) with or without UA. Animals were synchronized by bleaching or egg laying and grown on RNAi plates until they reached adult day 1, at which point assessments of swimming capacity and neuronal mitophagy were performed.

Mice

$SOD1^{G93A}$, $TDP43^{A315T}$, and rNLS8 transgenic mice were purchased from Jackson Laboratory (JAX stock Nos. 002726, 010700, and 028412). All mice were housed and bred in an environment with constant temperature and humidity, and a 12-hour light/dark cycle, at the Laboratory Animal Center of Sun Yat-sen University. Hemizygous female mice were used in our experiments, which were approved by the Institutional Animal Care and Use Committee of Sun Yat-sen University (SYSU-IACUC-2024-001144).

Drug administration in mice

UA (25 mg) was dissolved in 10 mL of 5% sodium carboxymethyl cellulose (Cmc-Na) using ultrasound to obtain a working solution of 2.5 mg/mL. It was administered by gavage at a dose of 50 mg/kg/day at 60 days of age. The weight of the mice was recorded daily until the experiment reached its terminal stage.

Neurological score

The neurological score was based on a 6-point scale from 0 to 5, as previously reported [23]: 0, a healthy mouse with no ALS-related symptoms; 1, tremors in the hind legs, defined as the onset of ALS; 2, mice showing difficulty separating the hind legs when suspended by their tails, indicating muscle weakness; 3, mice showing walking difficulty, either stumbling or wobbling; 4, mice unable to walk on all four legs, with their hind legs dragging; 5, mice that cannot right themselves within 30 seconds, defined as terminal-stage ALS. When the mice scored 4 points, a water bottle and food were placed in the cage to ensure that they could eat and drink normally. Mice with a score of 5 were euthanized for ethical reasons. Scores of the various groups were monitored and recorded daily.

Hanging wire test

This test evaluates limb motor function in mice. A barbed wire mesh 40 cm long, 30 cm wide, and 2 cm between wires was prepared and attached to a plastic housing cage of the same size. The wire was placed 50 cm above the bottom of the cage, which was covered with 2 cm of corncob bedding material to prevent injury. The mice were placed on the wire mesh, and the latency to fall was recorded. The maximum recording time was 180 s. Each mouse had three attempts. The time to fall was recorded weekly for the various groups.

Electrophysiological measurements by electromyography (EMG)

The compound motor action potential (CMAP) of the gastrocnemius muscle, elicited by sciatic nerve stimulation, was used to evaluate the functional status of the motor unit pool after drug administration for 30 days. The mice were anesthetized and placed on a warm plate at 37℃ before the electrophysiological test. Anesthesia was induced with 4% isoflurane and maintained with 2–3% isoflurane at an oxygen flow rate of 2.5 L/minute. The hair on the hind limbs and lower back was removed with depilatory cream to expose the sciatic notch and gastrocnemius muscle. Two ring electrodes were used for recording: electrode E1 was placed at the largest diameter of the gastrocnemius muscle, while reference electrode E2 was placed on the ipsilateral Achilles tendon. The skin under the electrodes was coated with conductive gel to reduce impedance. Two 33 G monopolar needles (Technomed) were used as cathode (S2) and anode (S1) for sciatic nerve stimulation. S1 was inserted into the subcutaneous tissue next to the ischiatic notch, and S2 was inserted into the subcutaneous tissue in the proximal ipsilateral hind limb, with a 5–8 mm gap between them. The surface ground electrode was placed on the animal's tail. The sciatic nerve was stimulated with square-wave pulses of 0.2 ms and intervals of 5,000 ms. The magnification was set to 0.1×. The low-pass filter was set to 20 Hz, and the high-pass filter to 10 kHz. The stimulus intensity started at 1.0 V and gradually increased until the amplitude reached a plateau. The CMAP amplitude was recorded at this point. The EMG equipment was purchased from iWorx Systems Inc.

Immunohistochemistry and image analysis

Immunohistochemistry used the following antibodies: ChAT (1:50; AB144P; Sigma), Parkin (1:50; PA5-13399; Thermo Fisher), p-ubiquitin (Ser65; 1:200; ab309155; Abcam), GFAP (1:400; 3670; Cell Signaling Technology), Iba-1 (1:300; 019-19741; Wako), LAMP1 (1:50; sc-19992; Santa Cruz), MTCO2 (1:200; 55070-1-AP; Proteintech), and secondary antibodies (Alexa Fluor 488 donkey anti-mouse, Alexa Fluor 555 donkey anti-rabbit, Alexa Fluor 488 donkey anti-goat) (1:300; 715-545-150, 711-565-152, and 705-545-147; Jackson ImmunoResearch).

Mice were anesthetized with 1.25% Avodin and perfused successively through the left ventricle with 0.9% normal saline and 4% paraformaldehyde in PBS (pH 7.4). The lumbar segment of the spinal cord was quickly removed and post-fixed for 8 hours. Subsequently, the segments were washed with PBS and processed in a sucrose gradient from 20% to 30%. Spinal cord tissues were embedded in optimal cutting temperature compound (OCT), sectioned at 20 μm, blocked with 10% donkey serum dissolved in 0.3% Triton X-100 for 60 minutes, and incubated overnight with the respective primary antibodies diluted in blocking buffer at 4°C. After washing in PBS, the sections were incubated with secondary antibodies at room temperature for 60 minutes and imaged using a Nikon microscope and an Olympus FV3000 confocal microscope. Representative images were selected based on their similarity to the group mean.

Antibody-specific detection

We utilized tissue-positive controls to validate antibody specificity. Staining was performed on tissues known to express the target protein. Observation of a clear signal confirmed the effectiveness of the staining procedure. To preclude nonspecific staining and background fluorescence, we omitted the primary antibody and incubated the sections with secondary antibodies directly after blocking. The absence of any positive signal in these samples confirmed that the signals in the final images originated solely from the specific binding between the primary antibodies and their respective targets.

Electron microscopy

Samples were prepared for electron microscopy as described previously [24]. Briefly, the mice were anesthetized and perfused through the left ventricle with 0.9% normal saline and a solution of 5% glutaraldehyde / 4% paraformaldehyde in PBS. The lumbar spinal cord was quickly removed and post-fixed in 5% glutaraldehyde at 4°C overnight. The samples were then washed with PBS and refixed in 1% OsO_4 at 4°C for 2 hours. Subsequently, the samples were dehydrated in an alcohol gradient from 30% to 100% and embedded in resin for ultrathin transverse sectioning. Sections were stained with lead citrate and uranyl acetate and scanned using a transmission electron microscope.

Autophagosomes were defined as double-layer membrane structures that encapsulated degenerated organelles, following the guidelines for the use and interpretation of assays for monitoring autophagy. Mitophagosomes were defined as autophagosomes containing damaged mitochondria. Autolysosomes were defined as organelles formed by the fusion of lysosomes and autophagosomes. Damaged mitochondria exhibited swelling, disappearance of internal cristae, and the appearance of giant cavities and vesicles, which accounted for more than 50% of the total area. The ratio of damaged mitochondria to all mitochondria, observed at high magnification, was used to evaluate the damage caused to the mitochondria [15]. The ratio of mitophagosomes to all damaged mitochondria was defined as the mitophagy index, indicating the level of mitophagy [15]. The sample size for this experiment (n = 3) was consistent with standards for neuronal ultrastructural analysis in research on other neurodegenerative diseases [25]. Representative images were selected based on their similarity to the group mean.

Western blot

The cell samples were processed quickly. RIPA lysis buffer (Thermo Fisher) containing protease and phosphatase inhibitors (Thermo Fisher) was used for sample homogenization. Protein concentration was assessed using the BCA protein assay (Thermo Fisher), followed by adding loading buffer containing 1% DTT (Thermo Scientific) for stabilization. All protein samples were stored at –80°C pending further use. Equal amounts of protein (30 μg) were separated on 10% or 12.5% SDS-PAGE (Bio-Rad), transferred onto 0.22-μm PVDF membranes (Merck Millipore), blocked with 5% bovine serum at room temperature for 1 hour, and incubated with primary antibodies diluted in TBST at 4°C overnight. These included p-ubiquitin Ser65 (1:1,000; 62802; Cell Signaling Technology), Parkin (1:1,000; 2132; Cell Signaling Technology), PINK1 (1:1,000; 6946; Cell Signaling Technology), mitofusin 2 (MFN2; 1:1,000; A19678; Abclonal), and β-actin (1:3,000; 4967; Cell Signaling Technology). After three washes with TBST, the PVDF membranes were incubated with HRP secondary antibodies (1:3,000; 7074; Cell Signaling Technology) at room temperature for 1 hour. The ECL reagent (Merck Millipore) was used for visualization, and the Asherman Imager 600 for imaging. For semiquantitative analysis, relative expression was calculated using β-actin as the internal reference for data normalization.

Statistical analysis

Technical replicates were used to ensure measurement precision and were averaged to represent a single value of each independent biological replicate before statistical analysis. All individual data points in the graphs represented biological replicates, which matched the n values reported in the corresponding figure legends. Data are presented as mean ± standard deviation (SD).

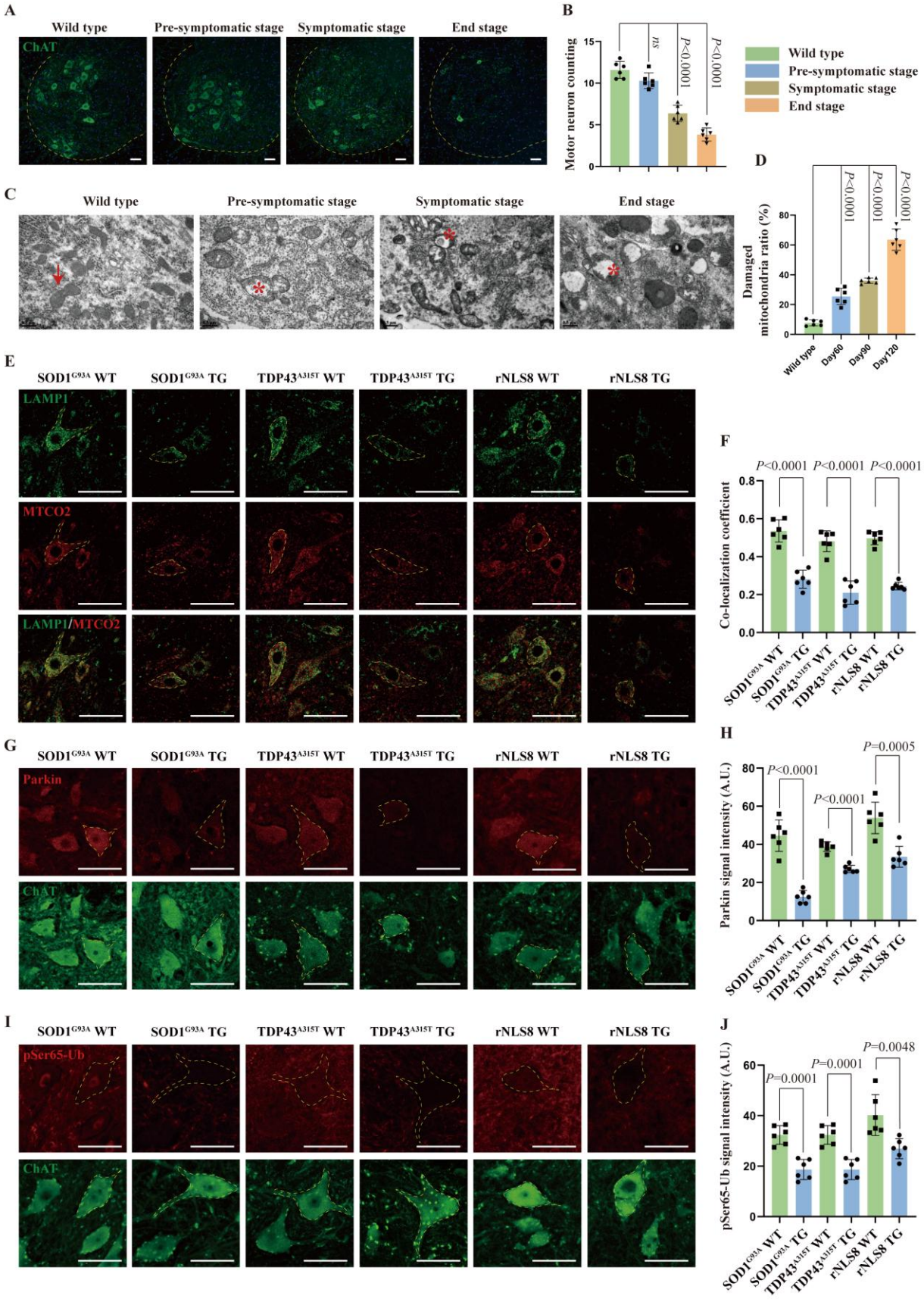
A
Wild type
Pre-symptomatic stage
Symptomatic stage
End stage
ChAT
B
Motor neuron counting
ns
P<0.0001
P<0.0001
Wild type
Pre-symptomatic stage
Symptomatic stage
End stage
C
Wild type
Pre-symptomatic stage
Symptomatic stage
End stage
D
Damaged mitochondria ratio (%)
P<0.0001
P<0.0001
P<0.0001
Wild type
Day60
Day90
Day120
E
SOD1G93A WT
SOD1G93A TG
TDP43A315T WT
TDP43A315T TG
rNLS8 WT
rNLS8 TG
LAMP1
MTCO2
LAMP1/MTCO2
F
Co-localization coefficient
P<0.0001
P<0.0001
P<0.0001
G
Parkin
ChAT
H
Parkin signal intensity (A.U.)
P=0.0005
P<0.0001
P<0.0001
I
pSer65-Ub
ChAT
J
pSer65-Ub signal intensity (A.U.)
P=0.0048
P=0.0001
P=0.0001

Figure 1. ALS mouse models show increased defective mitophagy with disease progression. (A and B) Motor neuron counts in three critical disease stages in the SOD1^{G93A} mouse model: a pre-symptomatic stage at 60 days of age, a symptomatic stage at 90 days of age, and a terminal end stage at 120 days of age. The number of motor neurons decreased significantly during the symptomatic stage. Scale bar = 50 μm. n = 6 animals/group. **(C and D)** Mitochondrial ultrastructure and mitophagy in SOD1^{G93A} and wild-type mice at the pre-symptomatic, symptomatic, and terminal end stages. Red arrows indicate normal mitochondria, and red asterisks indicate damaged mitochondria. Scale bar = 0.5 μm at 18,500× magnification. n = 6 animals/group. **(E and F)** Colocalization of mitochondrial marker protein MTCO2 and lysosomal marker protein LAMP2 in spinal motor neurons decreased in SOD1^{G93A}, TDP43^{A315T}, and rNLS8 mouse models. Scale bar = 50 μm. n = 6 animals/group. **(G and H)** Parkin expression in spinal motor neurons of SOD1^{G93A}, TDP43^{A315T}, and rNLS8 mouse models decreased at disease onset. Scale bar = 50 μm. n = 6 animals/group. **(I and J)** pSer65-Ub expression in spinal motor neurons of SOD1^{G93A}, TDP43^{A315T}, and rNLS8 mouse models decreased at disease onset. Scale bar = 50 μm. n = 6 animals/group. All individual data points in the graphs represented biological replicates, which matched the n values. Data are presented as means ± SD and were analyzed by Student's t-test for two independent samples, one-way ANOVA followed by turkey's post-hoc test for multiple samples.

The normality of data distribution was assessed using the Shapiro–Wilk test for all data. In our study, the data from experiments involving cells, nematodes, and animals were all found to be normally distributed. Accordingly, comparisons between two independent groups were performed using the Student's t-test. For comparisons among multiple groups, one-way ANOVA was applied, followed by Tukey's test for post hoc analysis. Survival curves for nematode lifespan, as well as mouse disease onset and lifespan were generated using the Kaplan-Meier method. The log-rank test was then employed to compare survival distributions between groups. Statistical significance was set at $P < 0.05$. Prism 9.0 (GraphPad Software, GA) and ImageJ were used for statistical analysis and image production.

RESULTS

Impaired mitophagy in spinal cord motor neurons in multiple mouse models of ALS

SOD1^{G93A} is established as the most classical animal model of ALS [26]. Three critical disease stages can be defined based on the number of spinal ChAT-positive motor neurons: a pre-symptomatic stage at 60 days of age, characterized by no motor neuron loss or behavioral changes; a symptomatic stage at 90 days of age, with motor neuron loss and symptomatic onset; and a terminal end stage at 120 days of age (Fig. 1A and B). Electron microscopy revealed a significant increase in mitochondrial ultrastructural abnormalities in spinal cord motor neurons of the SOD1^{G93A} mice as the disease progressed. These morphological alterations included marked mitochondrial swelling, the presence of vacuoles, and a conspicuous loss of inner cristae (Fig. 1C and D). The accumulation of damaged mitochondria suggests that the mitochondrial quality control system in ALS motor neurons is defective. Given that mitophagy selectively removes and recycles dysfunctional or superfluous mitochondria [9], these observations raise a key question: Is mitophagy impaired in motor neurons of ALS models, and does its impairment contribute to the accumulation of mitochondrial damage and subsequent neurodegeneration?

We combined another two ALS mouse models to further clarify whether neuronal mitophagy was impaired in ALS motor neurons by immunofluorescence. TDP43^{A315T} mouse model expresses the human mutant TDP-43 protein carrying the pathogenic A315T mutation associated with familial ALS and exhibits ALS-like symptoms typically between 120–150 days of age, including motor deficits and motor neuron loss [27]. The rNLS8 transgenic murine model employs a tetracycline (DOX)-regulated system to achieve inducible expression of human TDP43. Cytoplasmic mislocalization of the human TDP43 protein becomes detectable 7 days after DOX cessation, followed by ALS-like locomotor impairments by 14 days post-induction [28]. ChAT staining showed a significant motor neuron loss by day 120 in TDP43^{A315T} mice, while loss was observed 6 weeks after DOX withdrawal in rNLS8 mice (Supplementary Fig. 1A–D). When a significant loss of motor neurons was observed in the three mouse models, mitophagy levels were evaluated by examining the colocalization of the mitochondrial marker protein MTCO2 and the lysosomal marker protein LAMP2 in spinal ChAT-positive motor neurons. This analysis showed that mitophagy was significantly suppressed at the symptomatic stage (Fig. 1E and F). The consistent defect across models suggests that impaired mitophagy is a common hallmark of ALS and may be related to the accumulation of dysfunctional mitochondria and motor neuron loss.

Mitophagy comprises two independent but interrelated molecular pathways, among which the PINK1–Parkin-dependent pathway is the most classical and important [9]. Our findings indicate a profound disruption of this pathway in diseased motor neurons. The phosphorylation level of ubiquitin at Ser65 (the direct substrate level of PINK1) and the expression level of Parkin were reduced in spinal motor neurons of all three ALS mouse models (Fig. 1G–J). These data indicate a significant impairment of PINK1–Parkin-dependent mitophagy in ALS motor neurons. Considering the beneficial effects of maintaining normal mitochondrial

function in neurons, we investigated whether pharmacological activation of mitophagy could slow ALS progression.

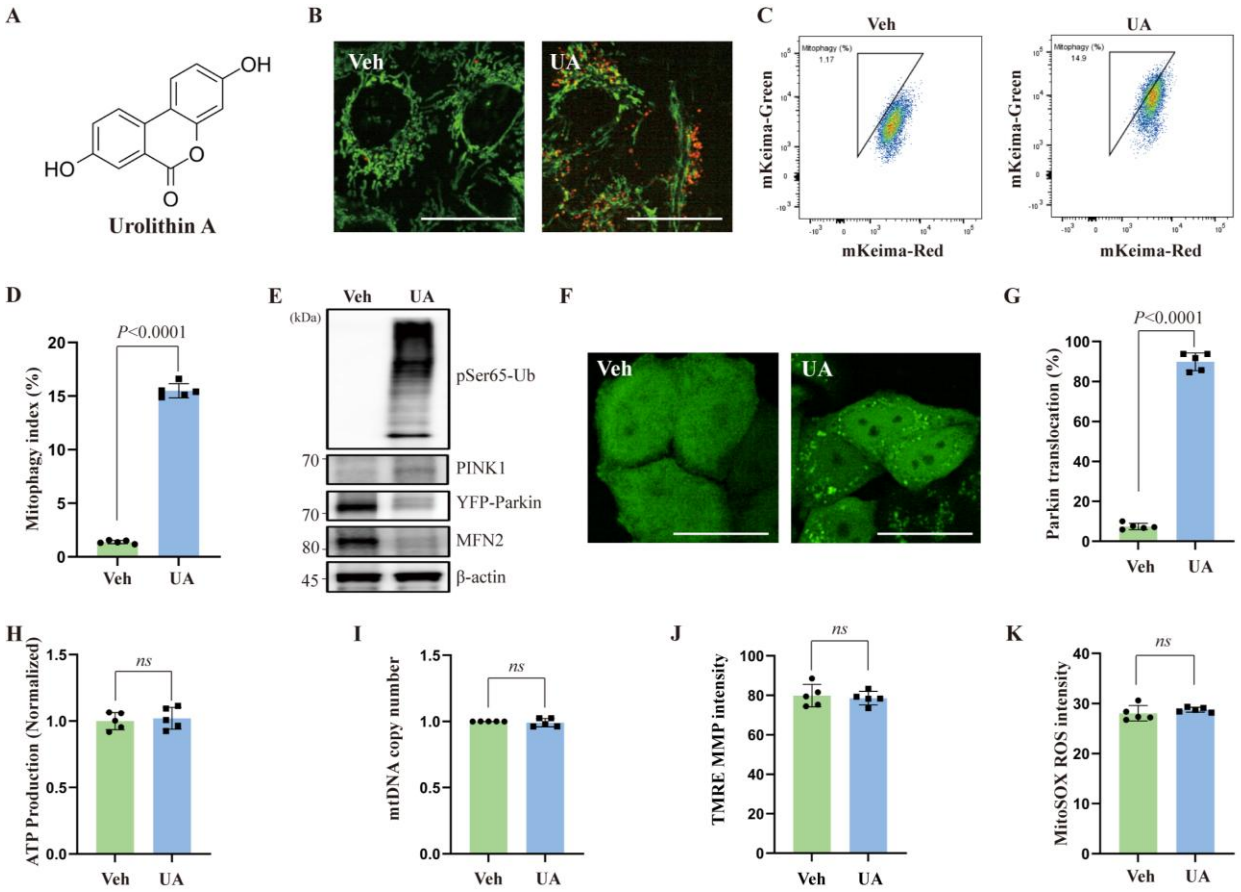

Figure 2. Urolithin A (UA) induces PINK1–Parkin-dependent mitophagy. (A) UA structure. **(B)** Living cell images of mt-mKeima staining showing mitophagy signals in YFP–Parkin–mito–Keima HeLa cells treated with UA (100 μM) for 24 hours. Scale bar = 50 μm. **(C)** Flow cytometric detection of mt-mKeima signals indicating mitophagy. **(D)** The statistical assessment of **(C)** showed that UA activated mitophagy. *n* = 5/group. **(E)** Immunoblot analysis of YFP–Parkin HeLa cells treated with UA. **(F)** Living cell images of UA-induced Parkin translocation in YFP–Parkin HeLa cells. Scale bar = 50 μm. **(G)** The statistical assessment of **(F)** showed that UA induced Parkin translocation. *n* = 5/group. **(H)** ATP production in the UA treatment group. *n* = 5/group. **(I)** qRT-PCR detection of mitochondrial DNA copy number in the UA treatment group. *n* = 5/group. **(J)** TMRE-labeled MMP in the UA treatment group. *n* =5 /group. **(K)** MitoSOX-labeled ROS levels in the UA treatment group. *n* = 5/group. All individual data points in the graphs represented biological replicates, which matched the *n* values. Data are presented as means ± SD and were analyzed by Student's *t*-test.

Pharmacological activation of PINK1–Parkin-dependent mitophagy

UA (Fig. 2A), a well-established mitophagy inducer [16], was selected to explore whether it could activate mitophagy and its molecular mechanism in mammalian cells using the Mito–Keima mitophagy reporter cell line. Keima is a pH-sensitive fluorescent protein activated at 440 nm in a neutral environment and 586 nm in an acidic environment. In the Mito–Keima HeLa cell line, the Keima protein is targeted to the mitochondria. The mitophagy level was inferred from the ratio of red-to-green fluorescence intensity [29]. In live-cell imaging and flow cytometry test, the red fluorescence intensity increased in Mito–Keima HeLa cells treated with UA, indicating mitophagy activation (Fig. 2B–D). Furthermore, immunoblot analysis revealed that treatment with 50 μM UA for 24 hours led to significant degradation of MFN2, an outer mitochondrial membrane protein (Fig. 2E). These data confirmed that UA is a potent mitophagy agonist.

As previously mentioned, mitophagy is mediated mainly through the PINK1–Parkin and receptor-mediated pathways [9]. We found that UA treatment markedly increased the expression of pSer65-Ub and PINK1 (Fig. 2E). Live-cell imaging showed that UA induced

substantial Parkin translocation (Fig. 2F and G), indicating enhanced Parkin E3 ligase activity. Accordingly, ubiquitination of MFN2, a known Parkin substrate, also increased in UA-treated cells (Fig. 2E). These results indicate that UA-activated mitophagy occurs via the PINK1–Parkin-dependent pathway.

To determine whether UA activates mitophagy through this pathway, siRNA was used to knock down PINK1 expression in YFP–Parkin and YFP–Parkin-Mito–Keima HeLa cells. When PINK1 expression was knocked down, UA-induced pSer65-Ub levels decreased (Supplementary Fig. 2A). Similarly, UA-induced Mito–Keima signals and Parkin translocation were inhibited (Supplementary Fig. 2B–E). These findings indicate that UA specifically stimulates PINK1–Parkin-dependent mitophagy.

We further evaluated key functional parameters to determine whether UA-induced mitophagy broadly disrupts mitochondrial physiology. No significant changes were observed in ATP production (Fig. 2H), mitochondrial DNA copy number (Fig. 2I), MMP (Fig. 2J), or cellular ROS levels (Fig. 2K). These results indicate that UA induces PINK1–Parkin-dependent mitophagy without compromising normal mitochondrial function, suggesting that UA may exert protective effects in disease contexts.

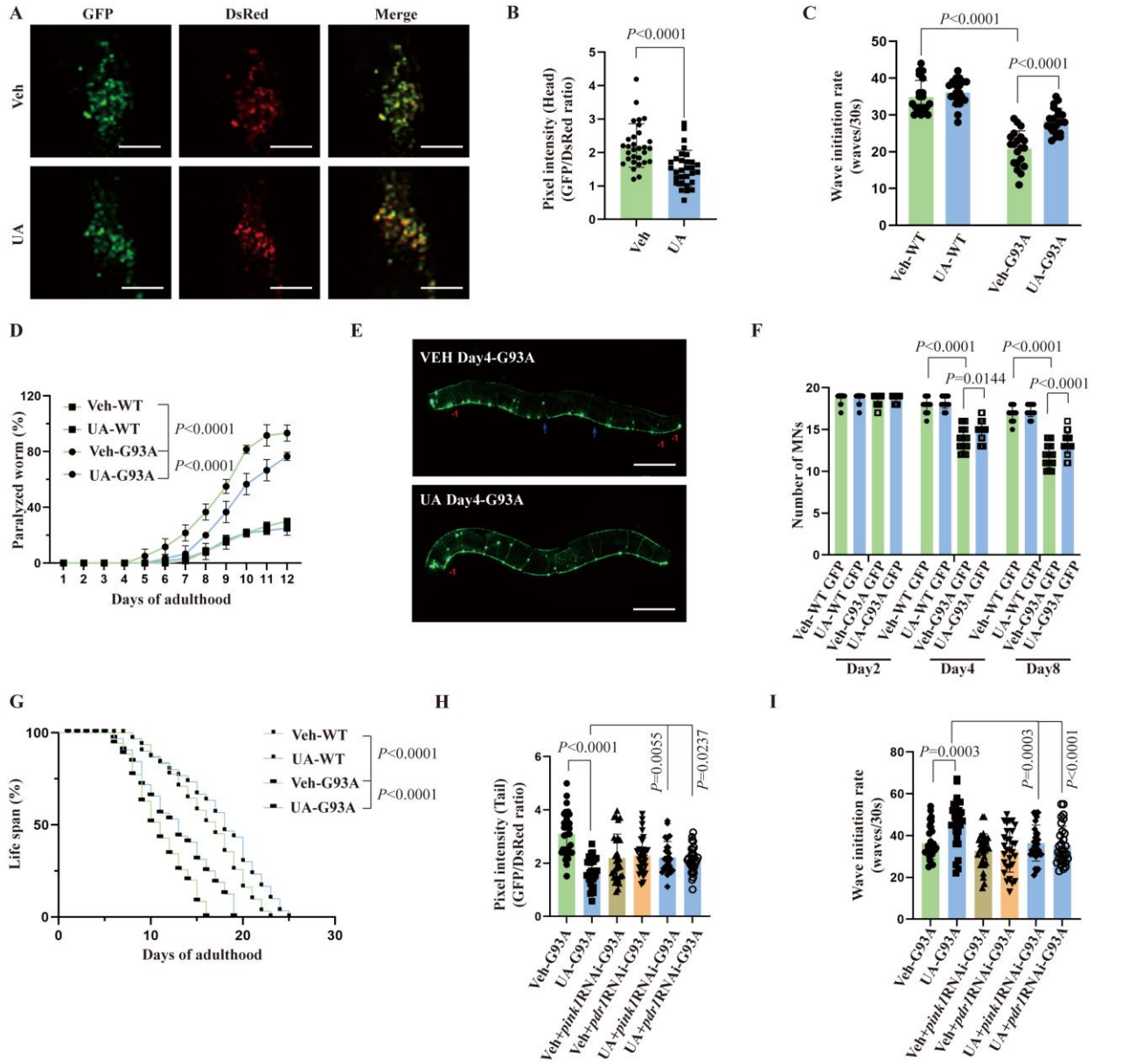

Figure 3. Mitophagy activation improves motor function in SOD1^{G93A} transgenic *C. elegans*. (A and B) Treatment with 100 μM UA significantly decreased the mt-Rosella GFP/DsRed ratio compared with the VEH group. Scale bar = 20 μm. *n* = 30

nematodes/group. **(C)** The SOD1^{G93A} transgenic nematodes demonstrated a significant decline in swimming ability compared with wild-type controls. Swimming ability improved after treatment with 100 μM UA. *n* = 20 nematodes/group. **(D)** The SOD1^{G93A} transgenic nematodes exhibited a significantly higher incidence of early-stage paralysis compared with wild-type controls. The onset of paralysis was delayed following treatment with 100 μM UA. *n* = 20 nematodes/group. **(E)** Motor neurons of a cross between SOD1^{G93A} and *unc25*::GFP nematodes on Day 4 of UA intervention were imaged by confocal microscopy. Red marker: motor neuron loss; blue marker: disrupted connections between motor neurons. Scale bar = 30 μm. **(F)** UA treatment (100 μM) significantly mitigated motor neuron loss in SOD1^{G93A} nematodes on Days 4 and 8 compared with untreated controls. *n* = 20 nematodes/group. **(G)** SOD1^{G93A} transgenic nematodes demonstrated a shorter lifespan compared with wild-type controls. UA treatment (100 μM) significantly prolonged their survival. *n* = 30 nematodes/group. **(H and I)** RNAi was used to knock down *pink-1* and *pdr-1* in MNs. TU3401 nematodes expressing SID-1 were crossed with each strain to ensure gene knockdown inside neurons. The positive effect of UA on neuronal mitophagy **(H)** and swimming ability **(I)** was inhibited by knockdown of *pink-1* and *pdr-1*. *n* = 30 nematodes/group. All individual data points in the graphs represented biological replicates, which matched the *n* values. Data are presented as means ± SD and were analyzed by Student's *t*-test for two independent samples, one-way ANOVA followed by turkey's post-hoc test for multiple samples. Survival curves for nematode lifespan were generated using the Kaplan-Meier method. The log-rank test was then employed to compare survival distributions between groups.

Pharmacological activation of mitophagy protects SOD1^{G93A} nematodes

Next, we explored the neuroprotective effect of mitophagy activation in SOD1^{G93A} *C. elegans*. To ensure that UA would not affect normal physiological processes, N2 wild-type Bristol isolate nematodes were used for toxicity assays, with 25, 50, 75, or 100 μM UA added to OP50/NGM plates. The four concentrations showed no significant differences from the control group in adult laying (Supplementary Fig. 3A), egg hatching efficiency (Figure S3B), L4 larval rate (Supplementary Fig. 3C), or adult number (Supplementary Fig. 3D). Moreover, 100 μM UA treatment for 12 days did not interfere with foraging behavior (Supplementary Fig. 3E). These results indicate that UA is non-toxic to nematodes at the concentrations tested; therefore, 100 μM was selected for subsequent experiments.

Neuronal mitochondria-targeted Rosella (mt-Rosella) transgenic nematodes, expressing a pan-neuronal mt-Rosella biosensor with a GFP variant sensitive to lysosomal acidity and a pH-insensitive Discosoma red fluorescent protein (DsRed), were used to detect neuronal mitophagy in *C. elegans* [30]. Under normal conditions, both GFP and DsRed signals were present in wild-type neurons, whereas treatment with 100 μM UA decreased the GFP/DsRed ratio (Fig. 3A and B), indicating effective stimulation of neuronal mitophagy *in vivo*.

We then used ALS SOD1^{G93A} transgenic nematodes to assess UA's neuroprotective effects. These nematodes exhibit several pathological features associated with human ALS, including progressive paralysis, loss of functional motor neurons (MNs), and neurodegeneration (Fig. 3C–G). Remarkably, exposure to 100 μM UA from egg hatching to adult day 1 significantly improved MN function, swimming ability, and paralysis in SOD1^{G93A} nematodes (Fig. 3C and D). *unc-25*::GFP nematodes were crossed with wild-type or G93A nematodes to label the MNs and their connections. Continuous exposure to 100 μM UA from egg laying to adult day 8 delayed MN loss and degeneration compared with the untreated controls (Fig. 3E and F). More importantly, UA improved the median survival of SOD1^{G93A} nematodes compared with controls (Fig. 3G). These results confirm that UA protects against MN degeneration in an *in vivo* nematode model of ALS.

To determine whether UA activates mitophagy via the PINK1–Parkin-dependent pathway *in vivo*, neuronal mt-Rosella transgenic nematodes with knockdown of neuronal *pink-1* (homolog of mammalian *PINK1*) or *pdr-1* (homolog of mammalian Parkin) were used. Knockdown of neuronal *pink-1* or *pdr-1* abolished UA-induced neuronal mitophagy (Fig. 3H), confirming that UA induces a pink1–pdr1-dependent mitophagy. Consistently, knockdown of neuronal *pink-1* and *pdr-1* abrogated UA's beneficial effects on swimming ability in SOD1^{G93A} and SID-1 nematodes (Fig. 3I). Collectively, these findings demonstrate that UA stimulates pink1–pdr1-dependent neuronal mitophagy in SOD1^{G93A} nematodes.

Pharmacological activation of mitophagy protects the SOD1^{G93A} mouse model

Because electrophysiological injury precedes symptom onset in SOD1^{G93A} transgenic mice, most studies select the pre-symptomatic stage (60 days) for therapeutic intervention [31]. We further investigated the therapeutic and protective effects of mitophagy activation in the ALS SOD1^{G93A} mouse model. UA was administered by gavage from Day 60 at a dose of 50 mg/kg/day until the terminal stage. Mouse weight was recorded daily, the hanging wire test was conducted weekly, and electrophysiological testing was performed after 30 days of UA administration. Tremors in the hind legs were defined as the disease onset. The Kaplan–Meier test showed that the mean time to tremor onset in the UA group (106.67 ± 10.89 days) was significantly later than in the control group (90.44 ± 5.53 days; Fig. 4A). However, UA at 50 mg/kg/day did not significantly prolong survival in SOD1^{G93A} mice (Fig.

4B). The neurological score in the UA group was lower than in controls from Day 91 onward (Fig. 4C). Hanging time in the hanging wire test was significantly longer in the treatment group than in controls during weeks 12–16 (Fig. 4D). UA also insignificantly delayed weight loss in the model mice (Fig. 4E). Electrophysiological testing showed that the CMAP amplitude in the UA group was higher than that in controls (Fig. 4F), suggesting that UA delayed CMAP decline after 30 days of treatment.

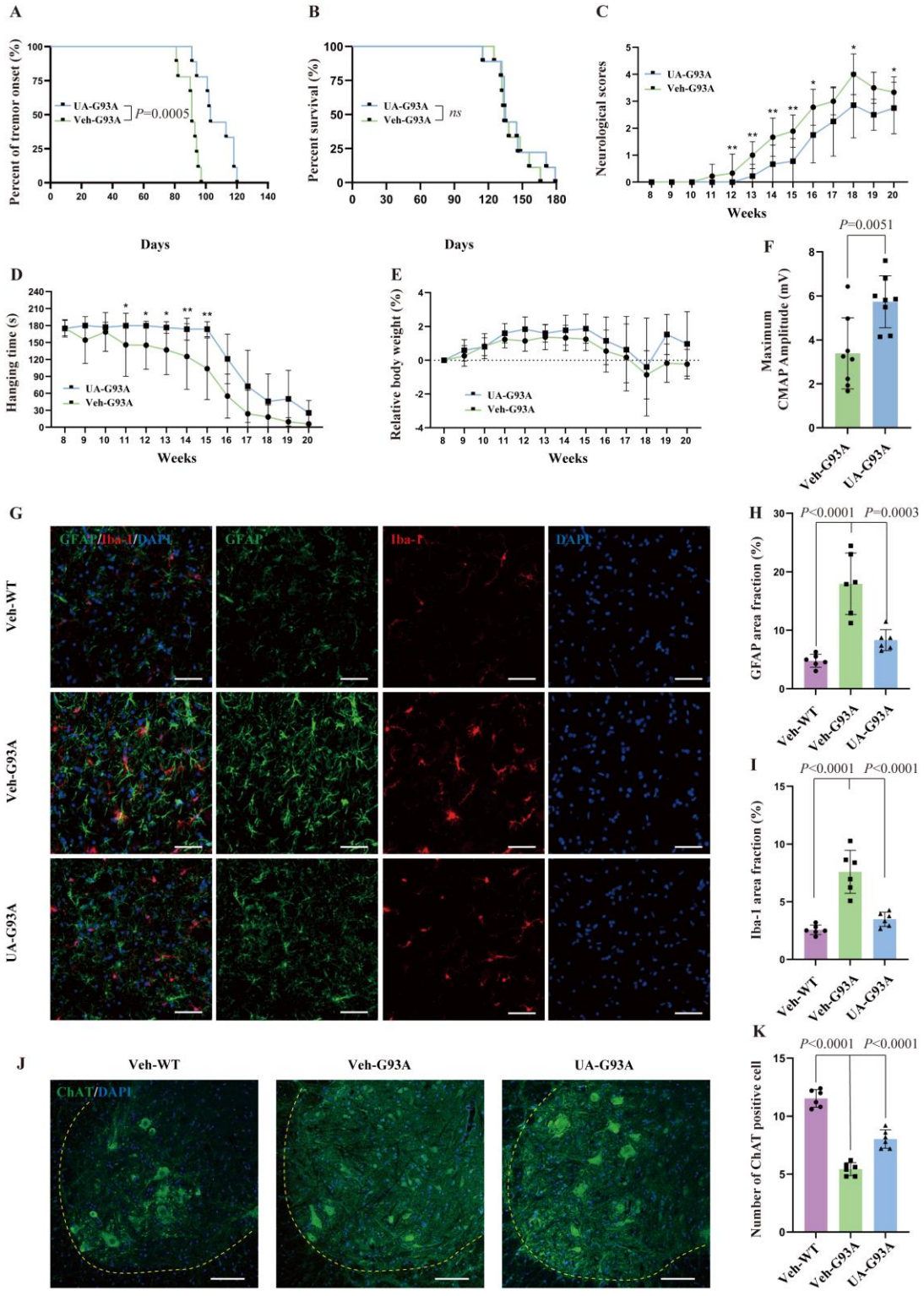

Figure 4. Pharmacological activation of mitophagy protects the SOD1^{G93A} mouse model. (A) UA treatment delayed disease onset in SOD1^{G93A} mice compared with controls. n = 8 animals/group. **(B)** UA did not prolong the survival of SOD1^{G93A} mice compared with controls. n = 8 animals/group. **(C)** The UA group had a lower neurologic score than the control group. n = 8 animals/group. **(D)** The hanging time of the UA group at 12–16 weeks of age was higher than in the control group. n = 8 animals/group. **(E)** UA insignificantly slowed weight loss in SOD1^{G93A} mice. n = 8 animals/group. **(F)** The CMAP amplitude of the gastrocnemius muscle following sciatic nerve stimulation in the UA group after 30 days of treatment was higher than in the control group. n = 8 animals/group. **(G–I)** Astrocyte proliferation and microglial activation in the anterior horn of the lumbar spinal cord after 30 days of UA treatment were decreased in SOD1^{G93A} mice. Scale bar = 50 μm. n = 6 animals/group. **(J and K)** UA treatment ameliorated motor neuron loss in the anterior horn of the lumbar spinal cord in SOD1^{G93A} mice. Scale bar = 50 μm. n = 6 animals/group. All individual data points in the graphs represented biological replicates, which matched the n values. Data are presented as means ± SD and were analyzed by Student's t-test for two independent samples, one-way ANOVA followed by turkey's post-hoc test for multiple samples. Survival curves for mouse disease onset and lifespan were generated using the Kaplan-Meier method. The log-rank test was then employed to compare survival distributions between groups. *P < 0.05, **P < 0.01, ***P < 0.001.

Spinal cords of SOD1^{G93A} mice showed high levels of neuroinflammation, including astrocyte proliferation and microglial activation (Fig. 4G–I). Pathological examination after 30 days of UA treatment showed reduced GFAP and Iba-1 fluorescence intensity in the anterior horn of the spinal cord (Fig. 4G–I), indicating that UA suppressed astrocyte proliferation and microglial activation. Neuronal degeneration was evident in solvent-treated control mice, particularly in the anterior horn of the lumbar spinal cord. In ALS, dying motor neurons typically exhibit abnormal morphology and vacuolar degeneration. The number of motor neurons in SOD1^{G93A} mice was significantly lower than in wild-type mice (Fig. 4J and K). Counting ChAT-positive neurons in the anterior horn of the spinal cord revealed that UA-treated SOD1^{G93A} mice had significantly higher number of surviving motor neurons (Fig. 4J and K).

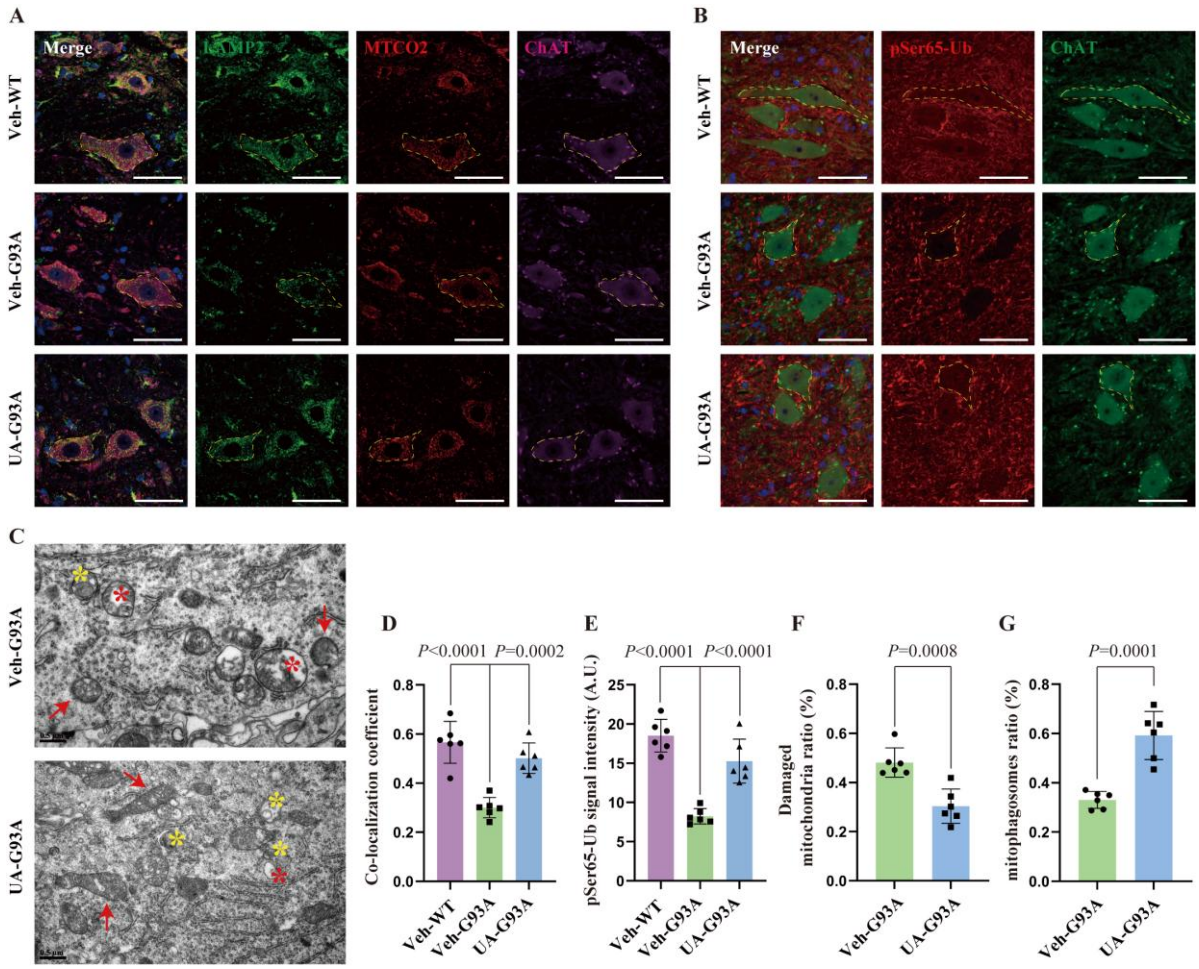

Figure 5. UA activates neuronal mitophagy via the PINK1–Parkin pathway in SOD1^{G93A} mice. (A and D) UA treatment significantly increased the colocalization of mitochondrial marker protein MTCO2 and lysosomal marker protein LAMP2 in spinal motor neurons. Scale bar = 50 μm. *n*=6 animals/group. **(B and E)** UA treatment significantly increased pSer65-Ub expression in spinal motor neurons. Scale bar = 50 μm. *n*=6 animals/group. **(C)** UA treatment improved mitochondrial ultrastructure in spinal motor neurons. Red arrows indicate normal mitochondria; red asterisks indicate damaged mitochondria; yellow arrows indicate lysosomes; and yellow asterisks indicate mitophagosomes. Scale bar = 0.5 μm at 18,500× magnification. **(F)** UA treatment significantly decreased the rate of damaged mitochondria in spinal motor neurons. *n*=6 animals/group. **(G)** UA treatment significantly increased the mitophagosome ratio in spinal motor neurons. *n*=6 animals/group. All individual data points in the graphs represented biological replicates, which matched the *n* values. Data are presented as means ± SD and were analyzed by Student's *t*-test for two independent samples, one-way ANOVA followed by turkey's post-hoc test for multiple samples.

UA activates neuronal mitophagy via the PINK1–Parkin pathway in SOD1^{G93A} mice

Colocalization of lysosomal and mitochondrial markers (LAMP2 and MTCO2, respectively) showed that UA treatment significantly increased their overlap compared with controls, indicating activation of mitophagy in spinal cord motor neurons in the ALS model **(**Fig. 5A and D). The expression level of pSer65-Ub, a direct substrate of PINK1, further indicated that UA significantly activated PINK1–Parkin-dependent mitophagy (Fig. 5B and E).

While immunofluorescence strongly suggested that UA affected mitophagy, transmission electron microscopy revealed corresponding ultrastructural improvements in motor neurons. UA-treated animals displayed mitochondria with more regular inner cristae and markedly reduced swelling and vacuolization (Fig. 5C). And the ratio of damaged mitochondria was significantly lower in the UA group than in the control group (Fig. 5F). Moreover, UA treatment significantly increased the mitophagosome ratio, indicating enhanced clearance of degenerated mitochondria through mitophagy (Fig. 5G). These findings suggest that UA protects ALS motor neurons by activating PINK1–Parkin-dependent mitophagy in the anterior horn of the spinal cord.

DISCUSSION

The current study confirmed the involvement of compromised mitophagy in motor neurons in ALS using mouse and *C. elegans* models with diverse genetic backgrounds. Similar results were reported in other studies that focused on motor neurons and NMJs [15]. Therefore, mitophagy could be a potential target to treat ALS. Here, we used the natural compound UA to activate PINK1–Parkin-dependent mitophagy, thereby removing damaged mitochondria and maintaining homeostasis. Mitophagy activation attenuated neuronal death and inhibited motor impairment in SOD1^{G93A} *C. elegans*. Our research proposes a new strategy for developing ALS drugs.

Despite differing genetic backgrounds and protein aggregation (e.g., SOD1, TDP43), multiple ALS models have consistently demonstrated mitochondrial dysfunction and mitophagy defects. From the perspective of mitochondrial homeostasis, impaired mitophagy may be related to mitochondrial dysfunction. Mitochondrial biosynthesis and clearance of damaged mitochondria constitute the mitochondrial quality control system. It was reported that protein aggregations directly inhibit the quality control mechanisms that maintain mitochondrial health [32]. Furthermore, damaged mitochondria trigger protective cellular responses, including PINK1–Parkin-dependent mitophagy. However, persistent and severe mitochondrial damage could overwhelm the quality control system, and chronic and excessive activation might lead to the exhaustion of this pathway [33].

Emerging evidence suggests that impaired mitophagy is a pathogenic hallmark in neurodegenerative diseases, while targeted modulation of this pathway holds great promise as a potential cure for these diseases [22]. Several studies have proposed strategies to induce mitophagy and demonstrated its neuroprotective effects in neurological disease models. For example, mitophagy activation suppresses inflammasome activation in Parkinson's disease [34]. Another study showed that NAD^+, a mitophagy inducer, reduced neuroinflammation and cell senescence in an Alzheimer's disease (AD) model [35]. Our study showed that treatment with UA increased the phosphorylation level of ubiquitin at Ser65 and altered Parkin, indicating that PINK1-dependent mitophagy was activated. While our *in vitro* and *C. elegans in vivo* findings provide direct evidence for pathway necessity, evidence based on colocalization and pSer65-Ub quantification in mouse models remains inferential. Therefore, future studies should employ conditional knockout models, utilizing techniques such as adeno-associated viruses with neuron-specific promoters or Cre recombinase technology, to obtain more direct evidence for UA-activated mitophagy *in vivo*. Moreover, the mechanisms by which UA induces neuronal mitophagy and how the activation of mitophagy ameliorates neurodegeneration require further in-depth research.

Although we have demonstrated that UA prolonged the survival of $SOD1^{G93A}$ transgenic nematodes and delayed disease onset while ameliorating motor deficits in $SOD1^{G93A}$ transgenic mice, it did not extend the overall survival of the mice. This outcome could have two main explanations. First, the multifaceted nature of ALS pathogenesis could account for the lack of survival benefits. Our data show that UA treatment effectively cleared damaged mitochondria and maintained mitochondrial homeostasis. However, as the disease progresses, multiple pathogenic mechanisms contribute to ALS pathogenesis, including excitotoxicity, oxidative stress, and neuroinflammation, collectively exacerbating motor neuron degeneration [36]. Second, although our results confirmed that UA delays motor neuron loss during the symptomatic phase of the disease, the pathology in the terminal stage may be too severe and irreversible for a single therapeutic strategy targeting mitophagy to counter. Therefore, optimizing dosing regimens and exploring combination therapies are critical next steps in related research.

UA is a highly promising therapeutic candidate for ALS as it has been shown to ameliorate mitochondrial pathology in ALS models by inducing PINK1–Parkin-dependent mitophagy. However, it was reported that UA also has therapeutic potential for aging-related disease, muscle dysfunction, and a broad spectrum of neurologic disorders [37]. UA also showed protective effects in models for ischemic stroke, multiple sclerosis, and muscular dystrophy [38-40]. Given UA's neuroprotective effects, several clinical trials have been initiated. Preliminary findings, particularly from those focusing on muscle strength and mitochondrial health, are promising [41, 42]. Importantly, UA is a metabolite of edible natural compounds. Our findings show that UA did not disrupt global mitochondrial function (e.g., ATP production and MMP), indicating that UA is safe for clinical application. Considering our results on UA application in ALS, future research should focus on the optimal therapeutic window during the early disease stage, as mitochondrial dysfunction is consistently an early event in disease progression. Moreover, based on our UA-derived data, we suggest that combining antioxidants and/or anti-excitotoxic agents with strategies that enhance mitophagy could yield additive, or even synergistic therapeutic benefits in patients with ALS.

This study focused on mitophagy—a selective type of autophagy that targets damaged mitochondria—and demonstrated that UA exerts neuroprotective effects by enhancing this process. UA could also enhance canonical autophagy. It was reported that UA is a novel activator of transcription factor EB (TFEB), inducing microglial autophagy and improving β-Amyloid (Aβ) degradation [43]. Moreover, a study on AD showed that UA could restore lysosomal function and ameliorate AD pathology [44]. Therefore, whether UA reduces SOD1 and TDP43 aggregation by enhancing autophagic and lysosomal functions warrants in-depth investigation. This will be the focus of our future research.

Our research also has some limitations. First, while our data suggest that impaired PINK1 – Parkin-dependent mitophagy is a shared feature across three mouse models of ALS, the efficacy of UA in activating mitophagy in TDP43-based models remains to be tested. Second, our study was conducted in female mice due to the aggressiveness of male $SOD1^{G93A}$ mice. Given that sex differences may affect the response to drug intervention, the efficacy of UA-related mitophagy activation in male mice should be supplemented in future studies.

Conclusion

This study delineated mitophagy dysregulation as a core pathogenic cascade in ALS and highlighted the potential mitophagy activation has in treating the disease. It will be interesting to continue studying various strategies to explore the therapeutic potential of mitophagy activation.

Acknowledgments

We thank our collaborators Prof. Le Weidong and Prof. Evandro Fei Fang for providing the transgenic nematodes strains used in this study. This study was supported by grants from the National Natural Science Foundation of China (82271448, 82471386), Guangdong Provincial Clinical Research Center for Neurological Diseases (2020 B1111170002), Guangdong Province International Cooperation Base for Early Intervention and Functional Rehabilitation of Neurological Diseases (2020A050502 0004), Guangzhou Major Difficult and Rare Diseases Project (2024MDRD02), Guangdong Provincial Engineering Center for Major Neurological Disease Treatment, Guangdong Provincial Translational Medicine Innovation Platform for Diagnosis and Treatment of Major Neurological Disease, Guangzhou Clinical Research and Translational Center for Major Neurological Diseases.

Conflicts of Interest

All authors declare that they have no conflicts of interest.

Supplementary Materials

The Supplementary data can be found online at: www.aginganddisease.org/EN/10.14336/AD.2025.1224.

References

[1] Brown RH, Al-Chalabi A (2017). Amyotrophic Lateral Sclerosis. N Engl J Med, 377:162-172.

[2] Lacomblez L, Bensimon G, Leigh PN, Guillet P, Meininger V (1996). Dose-ranging study of riluzole in amyotrophic lateral sclerosis. Amyotrophic Lateral Sclerosis/Riluzole Study Group II. Lancet, 347:1425-1431.

[3] (2017). Safety and efficacy of edaravone in well defined patients with amyotrophic lateral sclerosis: a randomised, double-blind, placebo-controlled trial. Lancet Neurol, 16:505-512.

[4] Al-Chalabi A, Hardiman O (2013). The epidemiology of ALS: a conspiracy of genes, environment and time. Nat Rev Neurol, 9:617-628.

[5] Taylor JP, Brown RH, Jr., Cleveland DW (2016). Decoding ALS: from genes to mechanism. Nature, 539:197-206.

[6] Hardiman O, Al-Chalabi A, Chio A, Corr EM, Logroscino G, Robberecht W, et al. (2017). Amyotrophic lateral sclerosis. Nat Rev Dis Primers, 3:17071.

[7] Sack MN, Fyhrquist FY, Saijonmaa OJ, Fuster V, Kovacic JC (2017). Basic Biology of Oxidative Stress and the Cardiovascular System: Part 1 of a 3-Part Series. J Am Coll Cardiol, 70:196-211.

[8] Pickles S, Vigié P, Youle RJ (2018). Mitophagy and Quality Control Mechanisms in Mitochondrial Maintenance. Curr Biol, 28:R170-r185.

[9] Fivenson EM, Lautrup S, Sun N, Scheibye-Knudsen M, Stevnsner T, Nilsen H, et al. (2017). Mitophagy in neurodegeneration and aging. Neurochem Int, 109:202-209.

[10] Lazarou M, Jin SM, Kane LA, Youle RJ (2012). Role of PINK1 binding to the TOM complex and alternate intracellular membranes in recruitment and activation of the E3 ligase Parkin. Dev Cell, 22:320-333.

[11] Pekkurnaz G, Wang X (2022). Mitochondrial heterogeneity and homeostasis through the lens of a neuron. Nat Metab, 4:802-812.

[12] Lin MT, Beal MF (2006). Mitochondrial dysfunction and oxidative stress in neurodegenerative diseases. Nature, 443:787-795.

[13] Mattiazzi M, D'Aurelio M, Gajewski CD, Martushova K, Kiaei M, Beal MF, et al. (2002). Mutated human SOD1 causes dysfunction of oxidative phosphorylation in mitochondria of transgenic mice. J Biol Chem, 277:29626-29633.

[14] Kong J, Xu Z (1998). Massive mitochondrial degeneration in motor neurons triggers the onset of amyotrophic lateral sclerosis in mice expressing a mutant SOD1. J Neurosci, 18:3241-3250.

[15] Rogers RS, Tungtur S, Tanaka T, Nadeau LL, Badawi Y, Wang H, et al. (2017). Impaired Mitophagy Plays a Role in Denervation of Neuromuscular Junctions in ALS Mice. Front Neurosci, 11:473.

[16] Picca A, Faitg J, Auwerx J, Ferrucci L, D'Amico D (2023). Mitophagy in human health, ageing and disease. Nat Metab, 5:2047-2061.

[17] Espín JC, Larrosa M, García-Conesa MT, Tomás-Barberán F (2013). Biological significance of urolithins, the gut microbial ellagic Acid-derived metabolites: the evidence so far. Evid Based Complement Alternat Med, 2013:270418.

[18] Heilman J, Andreux P, Tran N, Rinsch C, Blanco-Bose W (2017). Safety assessment of Urolithin A, a metabolite produced by the human gut microbiota upon dietary intake of plant derived ellagitannins and ellagic acid. Food Chem Toxicol, 108:289-297.

[19] Kujawska M, Jourdes M, Kurpik M, Szulc M, Szaefer H, Chmielarz P, et al. (2019). Neuroprotective Effects of Pomegranate Juice against Parkinson's Disease and Presence of Ellagitannins-Derived Metabolite-Urolithin A-In the Brain. Int J Mol Sci, 21.

[20] Yuan T, Ma H, Liu W, Niesen DB, Shah N, Crews R, et al. (2016). Pomegranate's Neuroprotective Effects against Alzheimer's Disease Are Mediated by Urolithins, Its Ellagitannin-Gut Microbial Derived Metabolites. ACS Chem Neurosci, 7:26-33.

[21] Li J, Li T, Zhang X, Tang Y, Yang J, Le W (2014). Human superoxide dismutase 1 overexpression in motor neurons of Caenorhabditis elegans causes axon guidance defect and neurodegeneration. Neurobiol Aging, 35:837-846.

[22] Fang EF, Hou Y, Palikaras K, Adriaanse BA, Kerr JS, Yang B, et al. (2019). Mitophagy inhibits amyloid-β and tau pathology and reverses cognitive deficits in models of Alzheimer's disease. Nat Neurosci, 22:401-412.

[23] Obrador E, Salvador R, Marchio P, López-Blanch R, Jihad-Jebbar A, Rivera P, et al. (2021). Nicotinamide Riboside and Pterostilbene Cooperatively Delay Motor Neuron Failure in ALS SOD1(G93A) Mice. Mol Neurobiol, 58:1345-1371.

[24] Ruffoli R, Bartalucci A, Frati A, Fornai F (2015). Ultrastructural studies of ALS mitochondria connect altered function and permeability with defects of mitophagy and mitochondriogenesis. Front Cell Neurosci, 9:341.

[25] Guo YS, Wu DX, Wu HR, Wu SY, Yang C, Li B, et al. (2009). Sensory involvement in the SOD1-G93A mouse model of amyotrophic lateral sclerosis. Exp Mol Med, 41:140-150.

[26] Oliván S, Calvo AC, Gasco S, Muñoz MJ, Zaragoza P, Osta R (2015). Time-Point Dependent Activation of Autophagy and the UPS in SOD1G93A Mice Skeletal Muscle. PLoS One, 10:e0134830.

[27] Hatzipetros T, Bogdanik LP, Tassinari VR, Kidd JD, Moreno AJ, Davis C, et al. (2014). C57BL/6J congenic Prp-TDP43A315T mice develop progressive neurodegeneration in the myenteric plexus of the colon without exhibiting key features of ALS. Brain Res, 1584:59-72.

[28] Walker AK, Spiller KJ, Ge G, Zheng A, Xu Y, Zhou M, et al. (2015). Functional recovery in new mouse models of ALS/FTLD after clearance of pathological cytoplasmic TDP-43. Acta Neuropathol, 130:643-660.

[29] Park K, Sonn SK, Seo S, Kim J, Hur KY, Oh GT, et al. (2023). Impaired TFEB activation and mitophagy as a cause of PPP3/calcineurin inhibitor-induced pancreatic β-cell dysfunction. Autophagy, 19:1444-1458.

[30] Cao SQ, Aman Y, Fang EF, Tencomnao T (2022). P. edulis Extract Protects Against Amyloid-beta Toxicity in Alzheimer's Disease Models Through Maintenance of Mitochondrial Homeostasis via the FOXO3/DAF-16 Pathway. Mol Neurobiol, 59:5612-5629.

[31] Mancuso R, Santos-Nogueira E, Osta R, Navarro X (2011). Electrophysiological analysis of a murine model of motoneuron disease. Clin Neurophysiol, 122:1660-1670.

[32] Briston T, Hicks AR (2018). Mitochondrial dysfunction and neurodegenerative proteinopathies: mechanisms and prospects for therapeutic intervention. Biochem Soc Trans, 46:829-842.

[33] Li A, Gao M, Liu B, Qin Y, Chen L, Liu H, et al. (2022). Mitochondrial autophagy: molecular mechanisms and implications for cardiovascular disease. Cell Death Dis, 13:444.

[34] Qiu J, Chen Y, Zhuo J, Zhang L, Liu J, Wang B, et al. (2022). Urolithin A promotes mitophagy and suppresses NLRP3 inflammasome activation in lipopolysaccharide-induced BV2 microglial cells and MPTP-induced Parkinson's disease model. Neuropharmacology, 207:108963.

[35] Hou Y, Wei Y, Lautrup S, Yang B, Wang Y, Cordonnier S, et al. (2021). NAD(+) supplementation reduces neuroinflammation and cell senescence in a transgenic mouse model of Alzheimer's disease via cGAS-STING. Proc Natl Acad Sci U S A, 118.

[36] Jiang S, Xu R (2025). The Current Potential Pathogenesis of Amyotrophic Lateral Sclerosis. Mol Neurobiol, 62:221-232.

[37] Wojciechowska O, Kujawska M (2023). Urolithin A in Health and Diseases: Prospects for Parkinson's Disease Management. Antioxidants (Basel), 12.

[38] Luan P, D'Amico D, Andreux PA, Laurila PP, Wohlwend M, Li H, et al. (2021). Urolithin A improves muscle function by inducing mitophagy in muscular dystrophy. Sci Transl Med, 13.

[39] Ahsan A, Zheng YR, Wu XL, Tang WD, Liu MR, Ma SJ, et al. (2019). Urolithin A-activated autophagy but not mitophagy protects against ischemic neuronal injury by inhibiting ER stress in vitro and in vivo. CNS Neurosci Ther, 25:976-986.

[40] Shen PX, Li X, Deng SY, Zhao L, Zhang YY, Deng X, et al. (2021). Urolithin A ameliorates experimental autoimmune encephalomyelitis by targeting aryl hydrocarbon receptor. EBioMedicine, 64:103227.

[41] Singh A, D'Amico D, Andreux PA, Fouassier AM, Blanco-Bose W, Evans M, et al. (2022). Urolithin A improves muscle strength, exercise performance, and biomarkers of mitochondrial health in a randomized trial in middle-aged adults. Cell Rep Med, 3:100633.

[42] Liu S, D'Amico D, Shankland E, Bhayana S, Garcia JM, Aebischer P, et al. (2022). Effect of Urolithin A Supplementation on Muscle Endurance and Mitochondrial Health in Older Adults: A Randomized Clinical Trial. JAMA Netw Open, 5:e2144279.

[43] Xiao Q, Wang J, Tian Q, Tian N, Tian Q, He X, et al. (2024). Uric Acid Mitigates Cognitive Deficits via TFEB-Mediated Microglial Autophagy in Mice Models of Alzheimer's Disease. Mol Neurobiol, 61:3678-3696.

[44] Hou Y, Chu X, Park JH, Zhu Q, Hussain M, Li Z, et al. (2024). Urolithin A improves Alzheimer's disease cognition and restores mitophagy and lysosomal functions. Alzheimers Dement, 20:4212-4233.